Active-matter isomorphs in the size-polydisperse Ornstein-Uhlenbeck Lennard-Jones model

Jespersen, Daniel; Costigliola, Lorenzo; Dyre, Jeppe C.; Saw, Shibu

Published in:
Journal of physics. Condensed matter : an Institute of Physics journal

DOI:
10.1088/1361-648X/aceac9

Publication date:
2023

Document Version
Publisher's PDF, also known as Version of record

Citation for published version (APA):
Jespersen, D., Costigliola, L., Dyre, J. C., & Saw, S. (2023). Active-matter isomorphs in the size-polydisperse Ornstein-Uhlenbeck Lennard-Jones model. *Journal of physics. Condensed matter : an Institute of Physics journal*, *35*(44), Article 445101. https://doi.org/10.1088/1361-648X/aceac9

Active-matter isomorphs in the size-polydisperse Ornstein–Uhlenbeck Lennard–Jones model

OPEN ACCESS
IOP Publishing
Journal of Physics: Condensed Matter
J. Phys.: Condens. Matter **35** (2023) 445101 (13pp)
https://doi.org/10.1088/1361-648X/aceac9

Active-matter isomorphs in the size-polydisperse Ornstein–Uhlenbeck Lennard–Jones model

Daniel Jespersen, Lorenzo Costigliola, Jeppe C Dyre* and Shibu Saw*

Glass and Time, IMFUFA, Department of Science and Environment, Roskilde University, PO Box 260, DK-4000 Roskilde, Denmark

E-mail: dyre@ruc.dk and shibus@ruc.dk

Received 16 May 2023, revised 18 July 2023
Accepted for publication 26 July 2023
Published 3 August 2023

Abstract

This paper studies size-polydisperse Lennard–Jones systems described by active Ornstein–Uhlenbeck particle (AOUP) dynamics. The focus is on the existence of isomorphs (curves of invariant structure and dynamics) in the model's three-dimensional phase diagram. Isomorphs are traced out from a single steady-state configuration by means of the configurational-temperature method. Good isomorph invariance of the reduced-unit radial distribution function and the mean-square displacement as a function of time is demonstrated for three uniform-distribution polydispersities, 12%, 23%, and 29%. Comparing to active-matter isomorphs generated by the analytical direct-isomorph-check method, the latter have poorer invariance of the structure, but better invariance of the dynamics. We conclude that both methods can be used to quickly get an overview of the phase diagram of polydisperse AOUP models involving a potential-energy function obeying the hidden-scale-invariance property required for isomorph theory to apply.

Keywords: Ornstein–Uhlenbeck model, active-matter isomorphs, active matter

(Some figures may appear in colour only in the online journal)

1. Introduction

Active matter involves particles that absorb energy from their environment and continuously perform motion dissipated into heat. This kind of motion, which in contrast to standard Newtonian or Brownian dynamics breaks time-reversal invariance [1, 2], is relevant not only for describing biological systems ranging from bacteria to flocking birds [3–10], but also for artificial microswimmers and active Janus particles.

Many different approaches to the description of active matter exist, depending on whether point particles or particles with directional coordinates are considered and depending on the precise mechanism by which the particles autonomously perform mechanical work [5, 6, 8, 9, 11, 12]. Point-particle active-matter models include the active Brownian particle (ABP) [13, 14] and active Ornstein–Uhlenbeck particle (AOUP) models; these have been used to describe the motion, e.g. in active colloids [15]. The AOUP model, which is simpler than the ABP model and has one less parameter, can be used to approximate ABP dynamics. Moreover, the AOUP model offers more possibilities to obtain theoretical predictions [16, 17]; this is the model we choose to study in the present paper. Specifically,

* Authors to whom any correspondence should be addressed.

the AOUP model involves point particles subject to a colored-noise Langevin dynamics [16, 18–20].

In view of the variability of biological and other active systems, it is not always realistic to assume all particles are identical. As a consequence, polydispersity has recently come into focus [21–24]. There is also currently a great deal of interest in passive polydisperse systems coming from, in particular, their use in SWAP-equilibrated supercooled liquids [25], in which context the question arises of how similar the dynamics of small and large particles are [26–28]. Finally, it is worth mentioning that active matter at high density has recently been studied inspired by biological materials such as cells, both for monodisperse [24, 29] and polydisperse cases [30], showing emerging collective phenomena with the spontaneous occurrence of spatial velocity correlations.

This paper studies the size-polydisperse AOUP Lennard–Jones (LJ) model. We recently demonstrated the existence of lines of approximately invariant structure and dynamics in the phase diagram of a binary LJ AOUP model; such lines are referred to as 'active-matter isomorphs' [31–33]. Inspired by the fact that the introduction of polydispersity into ordinary (passive) Newtonian models does not affect the existence of isomorphs [34], the present paper investigates whether the existence of isomorphs also survives the introduction of polydispersity into the AOUP model. This is important to investigate since the existence of isomorphs makes it possible to quickly establish an overview of the phase diagram because only a single point on each isomorph needs to be simulated.

2. The AOUP equation of motion and simulation details

We consider a system of N particles in volume V and define the (number) density by $\rho \equiv N/V$. If the potential-energy function is denoted by $U(\mathbf{R})$ in which $\mathbf{R} \equiv (\mathbf{r}_1, \ldots, \mathbf{r}_N)$ is the vector of all particle coordinates, the AOUP equation of motion [16, 18–20] is

$$\dot{\mathbf{R}} = -\mu \nabla U(\mathbf{R}) + \boldsymbol{\eta}(t)\,. \tag{1}$$

Here μ is the mobility (velocity over force) and the noise vector $\boldsymbol{\eta}(t)$ is colored according to an Ornstein–Uhlenbeck process, i.e. is a Gaussian stochastic process characterized by

$$\langle \eta_i^\alpha(t)\eta_j^\beta(t')\rangle = \delta_{ij}\delta_{\alpha\beta}\frac{D}{\tau}e^{-|t-t'|/\tau} \tag{2}$$

in which i and j are particle indices, α and β are xyz spatial indices, and D and τ are constants of dimension length squared over time and time, respectively.

We are interested in how the physics is affected when the density is changed, specifically in determining whether approximately invariant physics can be obtained by adjusting D and τ properly with density (μ is regarded as a material constant throughout). For the binary AOUP model this problem was studied in [32] that demonstrated how to change D and τ with density in order to achieve invariant structure and dynamics to a good approximation. The question is whether this is possible also for systems with a large uniform size polydispersity.

Table 1. Values of the polydispersity δ, σ range, and ratio between largest and smallest particle sizes for the three cases of uniform polydispersity studied.

δ	σ range	$\sigma_{\max}/\sigma_{\min}$
12%	0.80 − 1.20	1.50
23%	0.60 − 1.40	2.33
29%	0.50 − 1.50	3.00

In the AOUP model 'reduced' quantities are defined by using $l_0 = \rho^{-1/3}$ as the length unit and $t_0 = \tau$ as the time unit [32]. Reduced quantities are marked by a tilde. When we below speak about approximately invariant structure and dynamics, this particular state-point-dependent unit system is referred to.

We studied a system of $N = 5000$ particles in three dimensions interacting by LJ pair potentials, which between particles i and j are given by $v_{ij}(r) = 4\varepsilon\left[(r/\sigma_{ij})^{-12} - (r/\sigma_{ij})^{-6}\right]$ with $\sigma_{ij} = (\sigma_i + \sigma_j)/2$ (Lorentz–Berthelot mixing rule) and $\varepsilon = 1.0$. The particles sizes σ_i are distributed according to a uniform distribution with unity average. As usual, the polydispersity δ is defined by $\delta^2 = (\langle\sigma^2\rangle - \langle\sigma\rangle^2)/\langle\sigma\rangle^2$, which reduces to $\delta^2 = \langle\sigma^2\rangle - 1$. For the uniform distribution δ cannot exceed $1/\sqrt{3} \cong 58\%$. The three polydispersities studied below are $\delta \cong 11.5\%$, 23.1%, and 28.9%, corresponding to the size ranges listed in table 1 (these are for brevity henceforth reported as $\delta = 12\%$, 23%, and 29%). Note that the study thereby entails substantially different particle sizes, with the ratio of largest to smallest particle volume equal to 27 in the 29% polydispersity case.

All simulations used a shifted-force cutoff [35] of the ij particle interaction at the pair distance $r = 2.5\sigma_{ij}$ and the time step $\Delta t = \Delta\tilde{t}/(D\ \rho^{2/3})$ in which $\Delta\tilde{t} = 0.4$ [32]. The active-matter simulations were carried out on GPU cards using a home-made code, the MD simulations used RUMD [36].

3. Structure and dynamics along an isochore

Before discussing results for the variation of structure and dynamics along active-matter isomorphs, we briefly present analogous results along an isochore, i.e. for state points of same density. This sets the stage by illustrating that structure and dynamics do vary significantly throughout the (ρ, D, τ) AOUP phase diagram. Structure is studied by means of the average radial distribution function (RDF) denoted by $g(r)$. In figure 1(a) RDFs are shown along the $\rho = 0.85$ isochore for the $\delta = 29\%$ case (with values of D and τ taken from the $\delta = 29\%$ DIC active-matter isomorph studied below). Figure 1(b) shows the same data in reduced coordinates, which in this case simply

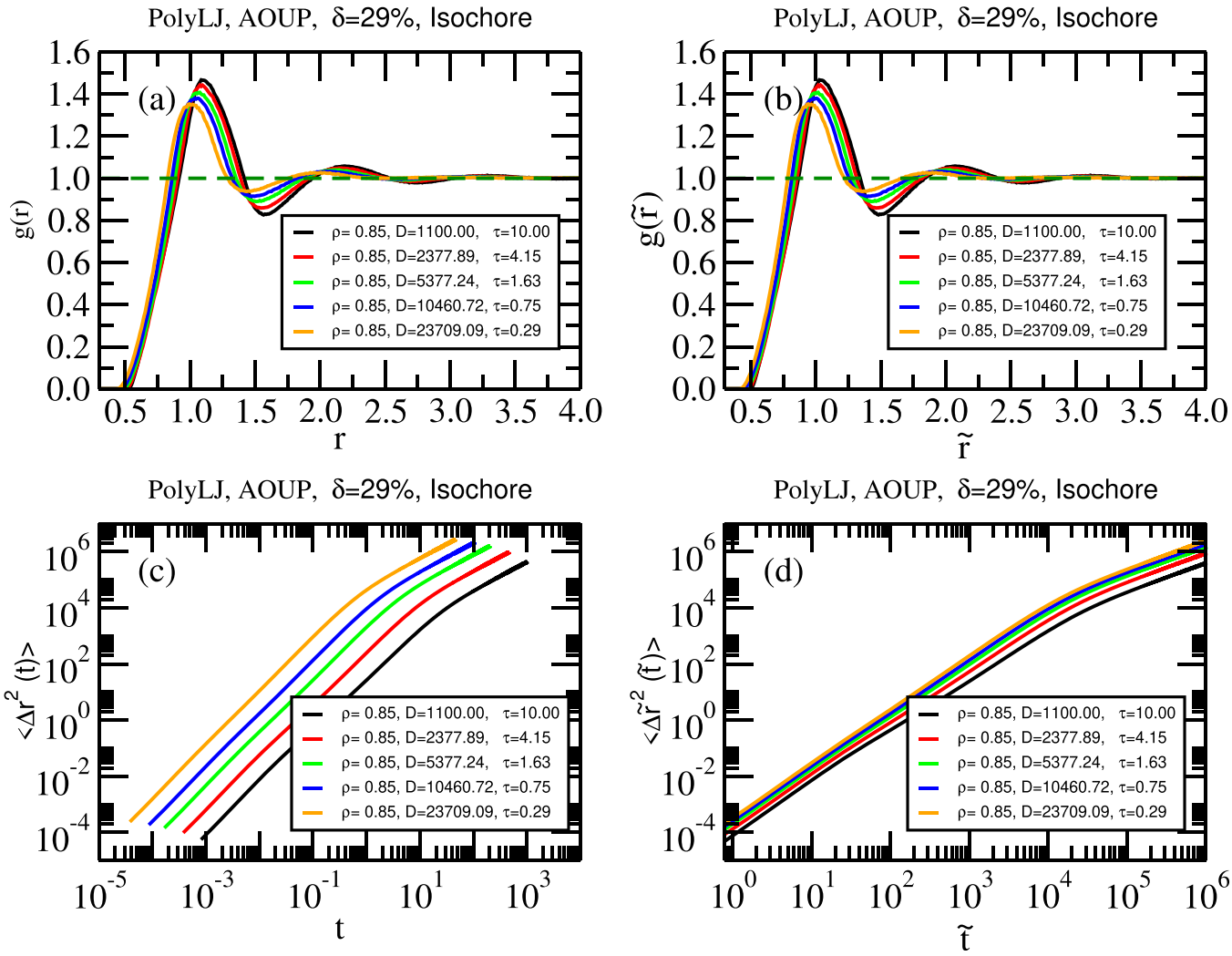

Figure 1. Average RDF and MSD for state points on the $\rho = 0.85$ isochore of the $\delta = 29\%$ polydispersity LJ AOUP model (the D and τ values are those of the below studied $\delta = 29\%$ active-matter DIC isomorph). (a) and (b) show the RDF as a function of the pair distance r and of the reduced pair distance $\tilde{r}$, respectively (the curves are the same because $\tilde{r} \propto r$ along an isochore). We see a substantial variation in the structure, with the most pronounced structure found for the smallest values D (black curve). The MSD likewise shows no collapse along the isochore, whether plotted (c) as a function of the time t or (d) as a function of the reduced time $\tilde{t}$. The slowest motion is found for the smallest D (black curve).

involves a common scaling of the x-coordinate. The parameters used in the simulations are listed in insets of the figures (more decimals of these parameters are provided in tables S1–S7 in the appendix).

We find a substantial structure variation along the isochore. The same applies for the mean-square displacement (MSD) as a function of the time t, $\langle \Delta r^2(t) \rangle$, which is plotted in a log-log plot in (c) LJ units and (d) reduced units. The short-time slope is two, reflecting the 'ballistic' regime of the AOUP model, which is absent in ordinary Langevin dynamics [16, 18–20] because it results from short-time noise correlations resulting in an inertia-like persistence of the direction of motion. At long times the well-known diffusive behavior leading to unity slope is observed. We note that the dynamics varies significantly along the isochore, whether or not given in reduced units.

4. Structure and dynamics along T_{conf}-generated active-matter isomorphs

Saw *et al* [32] used the configurational temperature T_{conf} for determining how to change the AOUP model parameters D and τ with density in order to achieve (approximately) invariant reduced structure and dynamics. The assumption is that $k_B T_{\text{conf}}$ is the relevant characteristic energy scale where T_{conf} is defined by $k_B T_{\text{conf}} \equiv \langle (\nabla U)^2 \rangle / \langle \nabla^2 U \rangle$ [37–39] in which k_B is the Boltzmann constant, ∇ is the gradient operator in the $3N$-dimensional configuration space, and the sharp brackets denote standard canonical-ensemble averages. In the thermodynamic limit the relative fluctuations of both the numerator and the denominator of T_{conf} go to zero. This implies that it is enough to consider a single configuration $\mathbf{R}_0$ using the expression $k_B T_{\text{conf}} \cong (\nabla U(\mathbf{R}_0))^2 / \nabla^2 U(\mathbf{R}_0)$.

The reasoning of [32] may be summarized as follows. Adopting $e_0 = k_B T_{\rm conf}$ as the energy unit supplementing the above introduced length and time units ($l_0 = \rho^{-1/3}$; $t_0 = \tau$), one first notes that the three quantities $\mu t_0 e_0/l_0^2$, Dt_0/l_0^2, and τ/t_0 are dimensionless. Assuming that these quantities cannot change with varying density if the structure and dynamics are invariant in reduced units, we conclude that $\mu \propto l_0^2/(t_0 e_0) = \rho^{-2/3}/(\tau k_B T_{\rm conf})$ and $D \propto l_0^2/t_0 = \rho^{-2/3}/\tau$. Since μ is assumed to be a material constant, this leads to $\tau \propto \rho^{-2/3}/k_B T_{\rm conf}$ and $D \propto k_B T_{\rm conf}$, i.e. to the following recipe for how D and τ changes with density from their values D_0 and τ_0 at a reference state point of density ρ_0:

$$D(\rho) = D_0 \frac{T_{\rm conf}(\rho)}{T_{\rm conf}(\rho_0)}\,,$$
$$\tau(\rho) = \tau_0 \left(\frac{\rho_0}{\rho}\right)^{2/3} \frac{T_{\rm conf}(\rho_0)}{T_{\rm conf}(\rho)}\,. \qquad (3)$$

For a large system $T_{\rm conf}(\rho_0)$ may as mentioned be evaluated from a single (steady-state) configuration, $T_{\rm conf}(\rho_0) \cong T_{\rm conf}(\mathbf{R}_0)$. Saw *et al* [32] demonstrated that this approximation introduces a negligible error for typical system sizes. In order to find $T_{\rm conf}(\rho)$ one scales $\mathbf{R}_0$ uniformly to the density ρ, i.e. substitutes $\mathbf{R} = (\rho_0/\rho)^{1/3}\mathbf{R}_0$ into the configurational temperature expression. This leads to

$$D(\rho) = D_0 \frac{T_{\rm conf}\left[(\rho_0/\rho)^{1/3}\mathbf{R}_0\right]}{T_{\rm conf}(\mathbf{R}_0)},$$
$$\tau(\rho) = \tau_0 \left(\frac{\rho_0}{\rho}\right)^{2/3} \frac{T_{\rm conf}(\mathbf{R}_0)}{T_{\rm conf}\left((\rho_0/\rho)^{1/3}\mathbf{R}_0\right)}\,. \qquad (4)$$

We used these equations for generating three active-matter isomorphs, starting in each case from the parameter values $D = 1100$ and $\tau = 10$ at the reference densities $\rho_0 = 0.99$, 0.91, and 0.85, respectively, for the polydispersities $\delta = 12\%$, 23%, and 29% (the reference densities were chosen to have the same virial, i.e. give the same contributions to the pressure coming from the interactions).

Results for the variation of the RDF are given in figure 2. The left column reports the RDF for the three polydispersities as functions of the pair distance r, the right column shows the same data as functions of the reduced pair distance $\tilde{r}$. In the latter case we find a good, though not perfect, data collapse and conclude that the average structure is approximately invariant along the active-matter isomorphs. In view of the fact that the density varies by a factor of two, this is not trivial.

Figure 3 shows analogous data for the MSD plotted in the same way with the left column giving the MSD as a function of time and the right column giving the same data in reduced units. There is a good data collapse with, however, a somewhat faster motion at the higher densities.

5. Comparing to direct-isomorph-check generated isomorphs

Above we demonstrated good invariance of the structure and dynamics along active-matter isomorphs generated by the $T_{\rm conf}$ method [32]. That method is easy to use and efficient because it requires just a single steady-state configuration at the reference state point to trace out the corresponding active-matter isomorph in the relevant phase diagram, *in casu* the (ρ, D, τ) diagram of the AOUP model. An alternative method for tracing out active-matter isomorphs is the analytical 'direct isomorph-check' (DIC) method, which in the appendix of [32] was shown to result in somewhat better isomorph-invariance of the dynamics of the AOUP Kob–Andersen binary LJ model.

Consider first a standard passive Newtonian systems involving LJ pair interactions of any kind, i.e. single-component, binary, or polydisperse systems, defined by some mixing rule. For such a system the analytical DIC recipe for tracing out a standard (passive) equilibrium isomorph [40, 41] is

$$\frac{h(\rho)}{T} = \text{Const.} \qquad (5)$$

Here $h(\rho)$ is the following function of density [40, 41]

$$h(\rho) = \left(\frac{\gamma_0}{2} - 1\right)\left(\frac{\rho}{\rho_0}\right)^4 - \left(\frac{\gamma_0}{2} - 2\right)\left(\frac{\rho}{\rho_0}\right)^2 \qquad (6)$$

in which ρ_0 is the reference-state-point density and γ_0 is the density-scaling exponent at the reference state point. This exponent can be determined numerically by means of

$$\gamma_0 = \frac{\langle \Delta U \Delta W \rangle}{\langle (\Delta U)^2 \rangle}\,. \qquad (7)$$

in which ΔW and ΔU are the deviations from the equilibrium values of virial and potential energy, respectively, and the angular brackets denote standard *NVT* equilibrium averages [31, 42].

For any system (passive or active, equilibrium or non-equilibrium) the systemic temperature $T_{\rm s}(\mathbf{R})$ is defined as the temperature of the corresponding thermal-equilibrium Newtonian system at the state point with the density of the configuration $\mathbf{R}$ and average potential energy equal to $U(\mathbf{R})$ [43]. In the thermodynamic limit fluctuations in $T_{\rm s}(\mathbf{R})$ go to zero, implying that one has at any time a well-defined systemic temperature $T_{\rm s}$. For, e.g. a driven passive or an active-matter system, a 'systemic isomorph' is defined as a curve in the $(\rho, T_{\rm s})$ phase diagram identical to an isomorph in the standard equilibrium Newtonian (ρ, T) phase diagram [43]. Thus in the analytical DIC, the systemic-temperature's variation with density is given by

$$\frac{h(\rho)}{T_{\rm s}(\rho)} = \text{Const.}\,, \qquad (8)$$

i.e. $T_{\rm s}(\rho) \propto h(\rho)$. The analytical DIC method for generating an active-matter isomorph of the AOUP model is arrived at

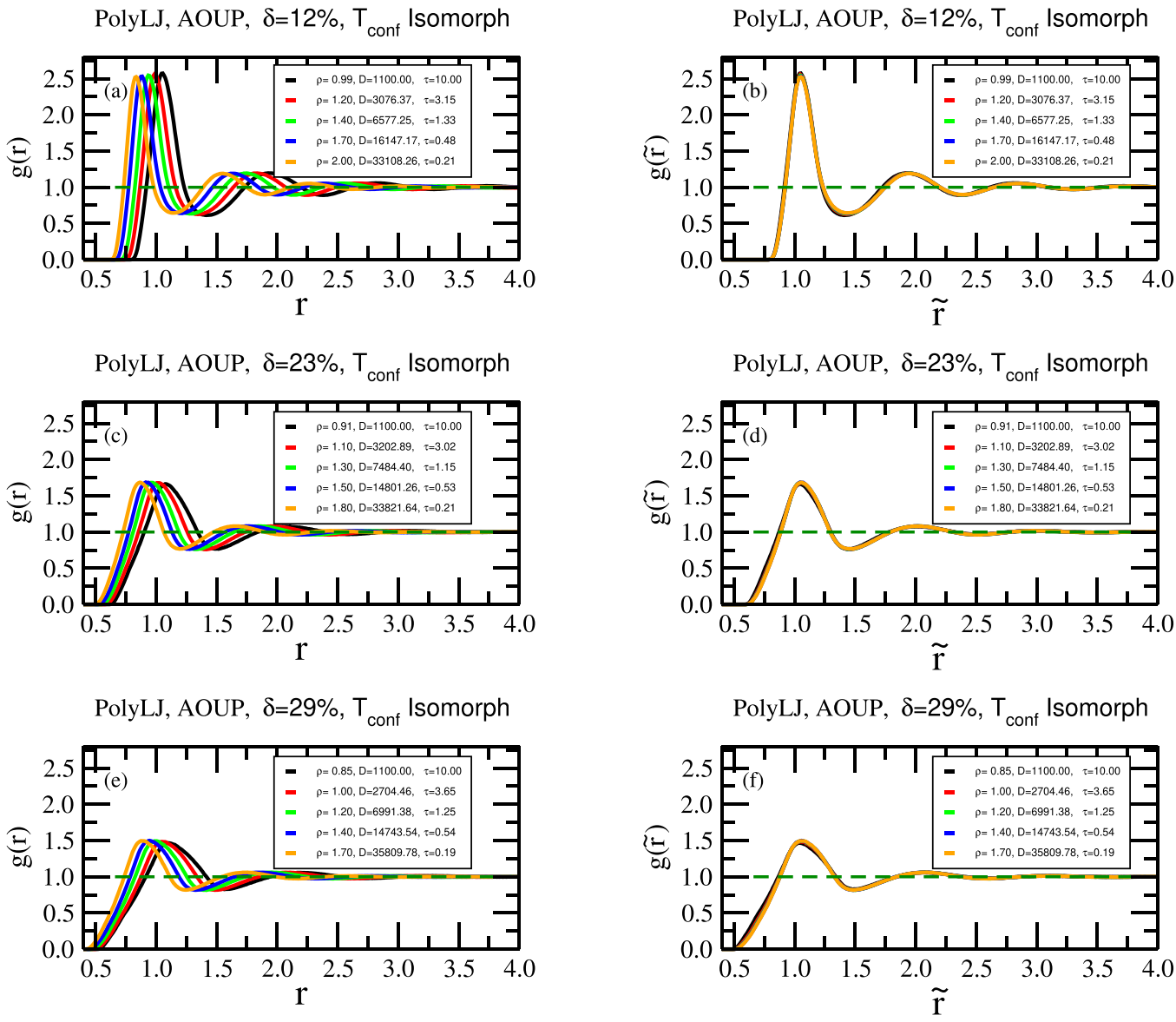

Figure 2. Structure probed along $T_{\rm conf}$-generated active-matter isomorphs. (a), (c), and (e) show the (average) RDFs for polydispersity $\delta = 12\%$, 23%, and 29%, respectively, while (b), (d), and (f) show the same data as functions of the reduced pair distance $\tilde{r}$. In all three cases we see a good collapse of the reduced RDF along the active-matter isomorph.

by replacing the configurational temperature in equation (3) by the systemic temperature $T_{\rm s}$ (this procedure was justified in [32]). Via equation (8) this leads to

$$D(\rho) = D_0 \frac{h(\rho)}{h(\rho_0)}\,,$$
$$\tau(\rho) = \tau_0 \left(\frac{\rho_0}{\rho}\right)^{2/3} \frac{h(\rho_0)}{h(\rho)}\,. \qquad (9)$$

Table 2 reports the systemic temperatures at the reference state points of the three polydispersities studied. As mentioned, the reference densities were chosen to have the same virial; we see that they also have almost the same systemic temperature.

Figure 4 shows the active-matter isomorph obtained from the $T_{\rm conf}$ method (full curves) and the analytical DIC method (dashed curves), starting at the reference state point $(\rho, D, \tau) = (\rho_0, 1100, 10)$ in which the reference density is 0.99, 0.91, and 0.85, respectively, for $\delta = 12\%$, 23%, and 29%. The two methods for generating isomorphs result in visibly different curves; thus there is more than 50% difference in D and τ at the largest density in the 29% polydispersity case (green curves). How different are these active-matter isomorphs when it comes to average RDF and MSD data collapse? The RDF case is investigated in figure 5, which shows that the structure is somewhat more invariant along the $T_{\rm conf}$-generated active-matter isomorphs than along the DIC-generated isomorphs, albeit this is a minor effect because in both cases the structure is quite

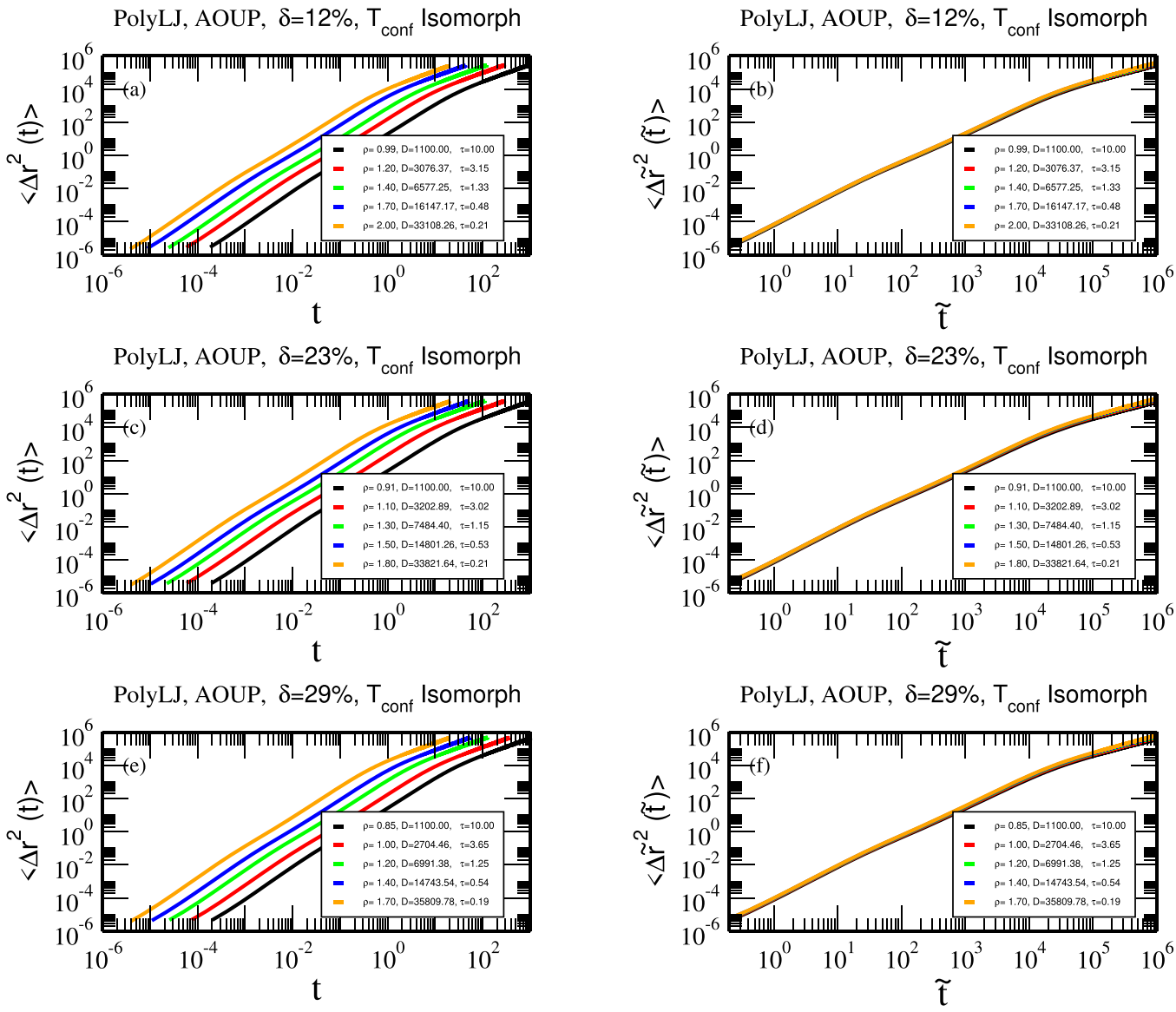

Figure 3. Dynamics probed along $T_{\rm conf}$-generated active-matter isomorphs. (a), (c), and (e) show the MSDs for polydispersity $\delta = 12\%$, 23%, and 29%, respectively, as functions of time, while (b), (d), and (f) show the same data in reduced units. There is a good, but not perfect, collapse of the reduced MSD along the active-matter isomorphs.

Table 2. Systemic temperature $T_{\rm s}$ and average potential energy $\langle U \rangle$ at the reference densities ρ_0 of the three polydisperse systems studied. In all three cases the values of the AOUP parameters at the reference densities are $D = 1100$ and $\tau = 10$.

ρ_0	δ	T_s	$\langle U \rangle$
0.990	12%	0.96	−4.455
0.905	23%	0.98	−4.447
0.850	29%	1.00	−4.321

invariant. The differences are most pronounced at higher polydispersity.

Figure 6 reports results for the MSD. Here we reach the opposite conclusion: the DIC method results in a somewhat better data collapse than the $T_{\rm conf}$ method. The same conclusion was reached for the binary Kob–Andersen AOUP model in [32] (that did not investigate the average RDF).

6. Role of smallest and largest particles

To illuminate why the structure is not always isomorph invariant, we studied for the 29% polydispersity simulation data the structure and dynamics of the 20% smallest and largest particles along the DIC isomorph (figure 7). The RDF is here defined by limiting the central particle to be either among the

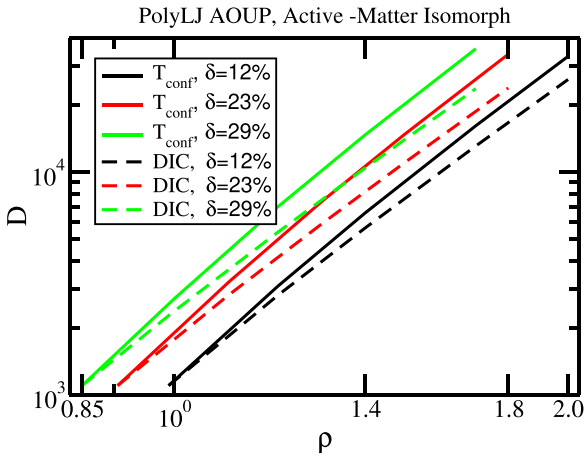

Figure 4. Active-matter isomorphs for the polydispersities $\delta = 12\%$, 23%, and 29%, generated from the reference state points by two different methods, the $T_{\rm conf}$ method of section 4 (full curves) and the analytical DIC method (dashed curves). The isomorphs are visibly different.

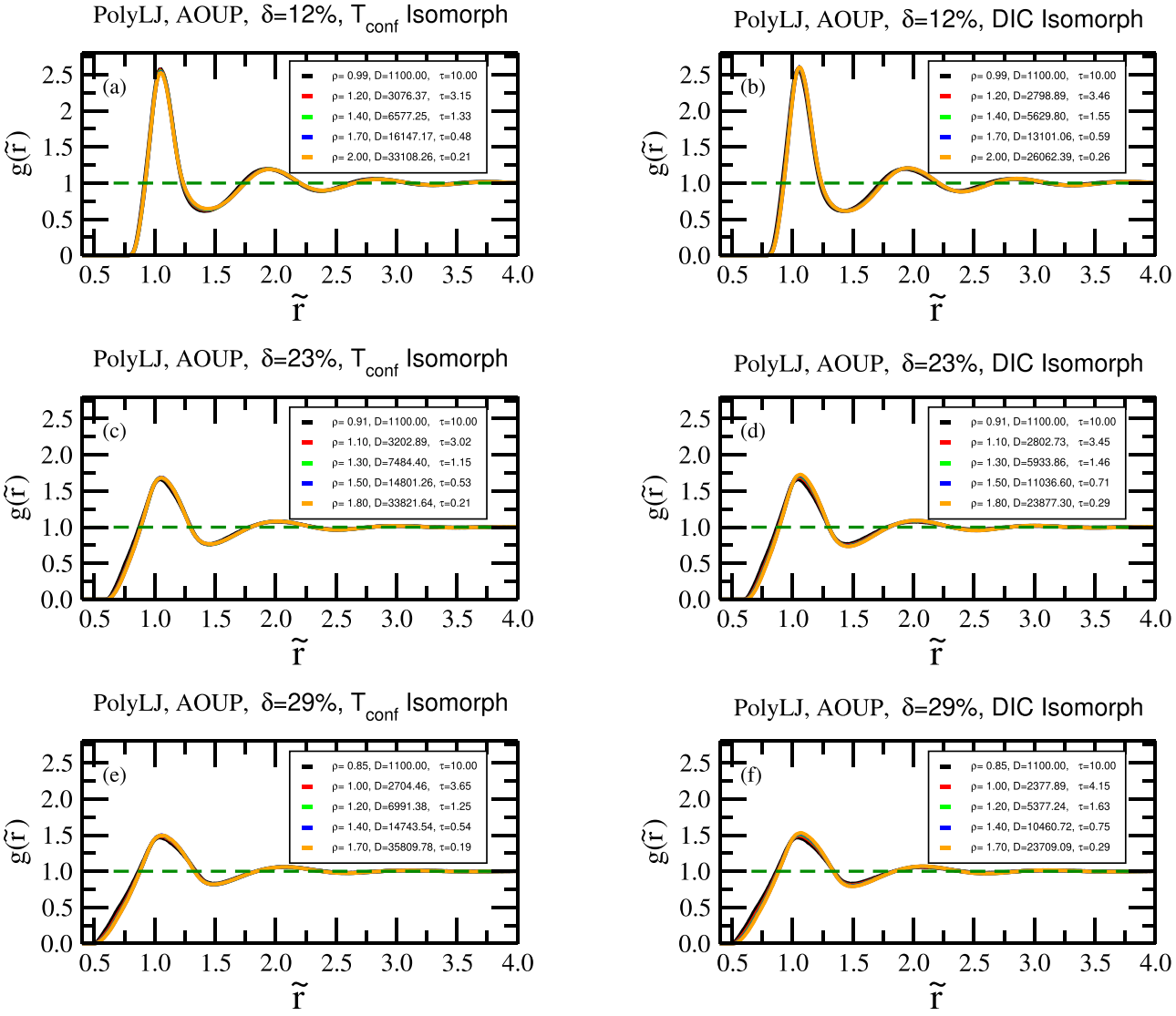

Figure 5. Comparing the degree of structural invariance along $T_{\rm conf}$-generated and DIC-generated active-matter isomorphs. (a), (c), and (e) show the reduced average RDFs for polydispersity $\delta = 12\%$, 23%, and 29%, along the $T_{\rm conf}$-generated isomorphs, while (b), (d), and (f) show the corresponding reduced average RDFs along the DIC-generated isomorphs. There is a slightly better data collapse along the $T_{\rm conf}$-generated isomorphs.

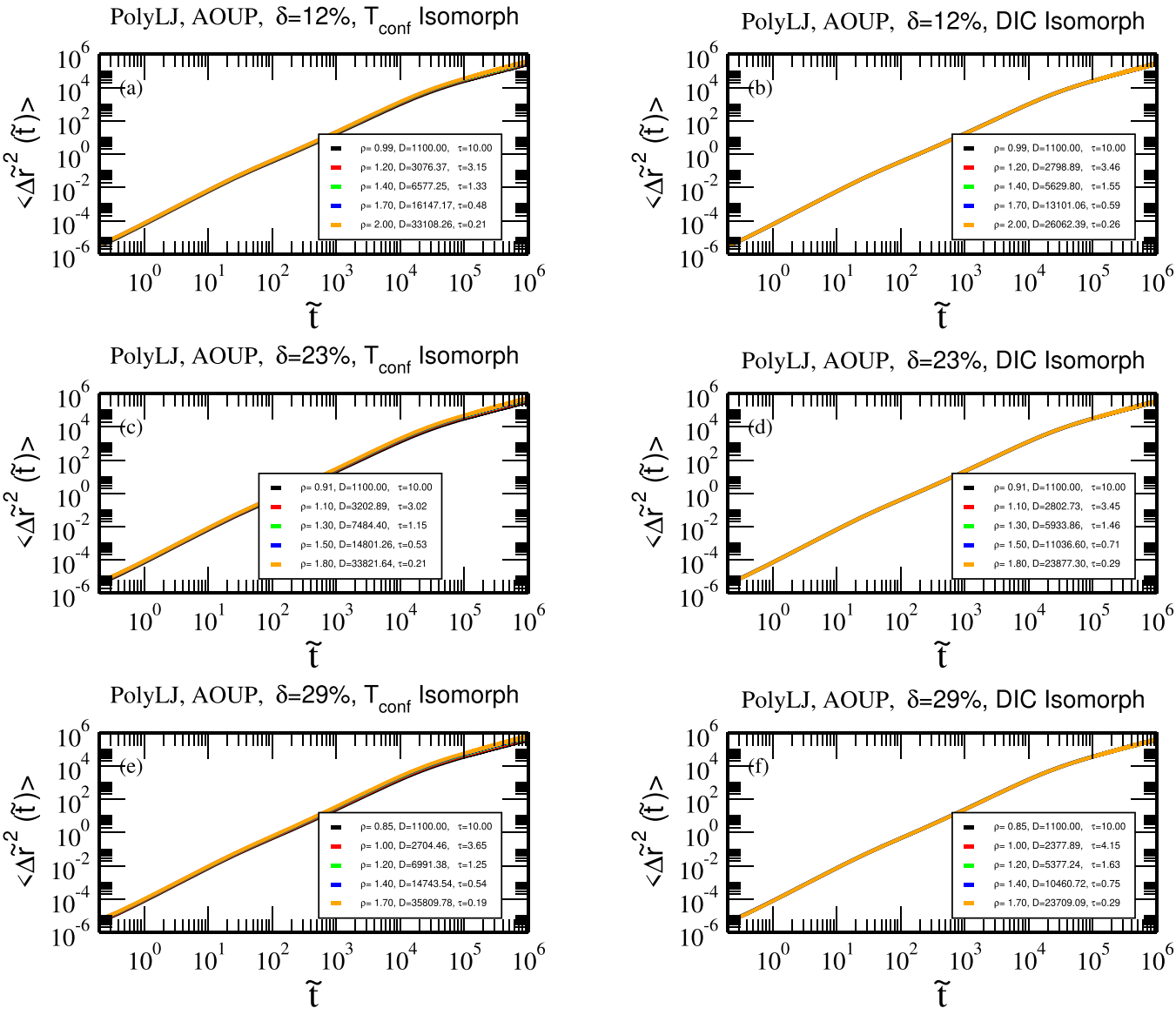

Figure 6. Comparing the degree of invariance of the dynamics along the $T_{\rm conf}$-generated and DIC-generated active-matter isomorphs. (a), (c), and (e) show the reduced MSDs for polydispersity $\delta = 12\%$, 23%, and 29%, along the $T_{\rm conf}$-generated isomorphs, while (b), (d), and (f) show the corresponding reduced MSDs along the DIC-generated isomorphs. There is a better data collapse along the DIC-generated isomorphs.

smallest or among the largest 20% and counting only neighboring particles of the same kind. In both cases, the peaks are narrower and higher than that of the average RDF (figure 5(f)), which reflects the limitation to similar-sized particles. We note that unlike in figure 5(f), in figure 7(a) the most pronounced structure is seen at the lowest density. Interestingly, the structure around the smallest particles is not DIC-isomorph invariant, while that around the largest particles is; a similar result applies for the $T_{\rm conf}$-generated isomorph (data not shown). In contrast to the findings for structure, the dynamics of both small and large particles is DIC-isomorph invariant to a good approximation, even though the small particles move considerably faster than the large. We conclude that the lack of perfect isomorph invariance of the overall RDF largely reflects the fact that the structure around the smallest particles is not isomorph invariant.

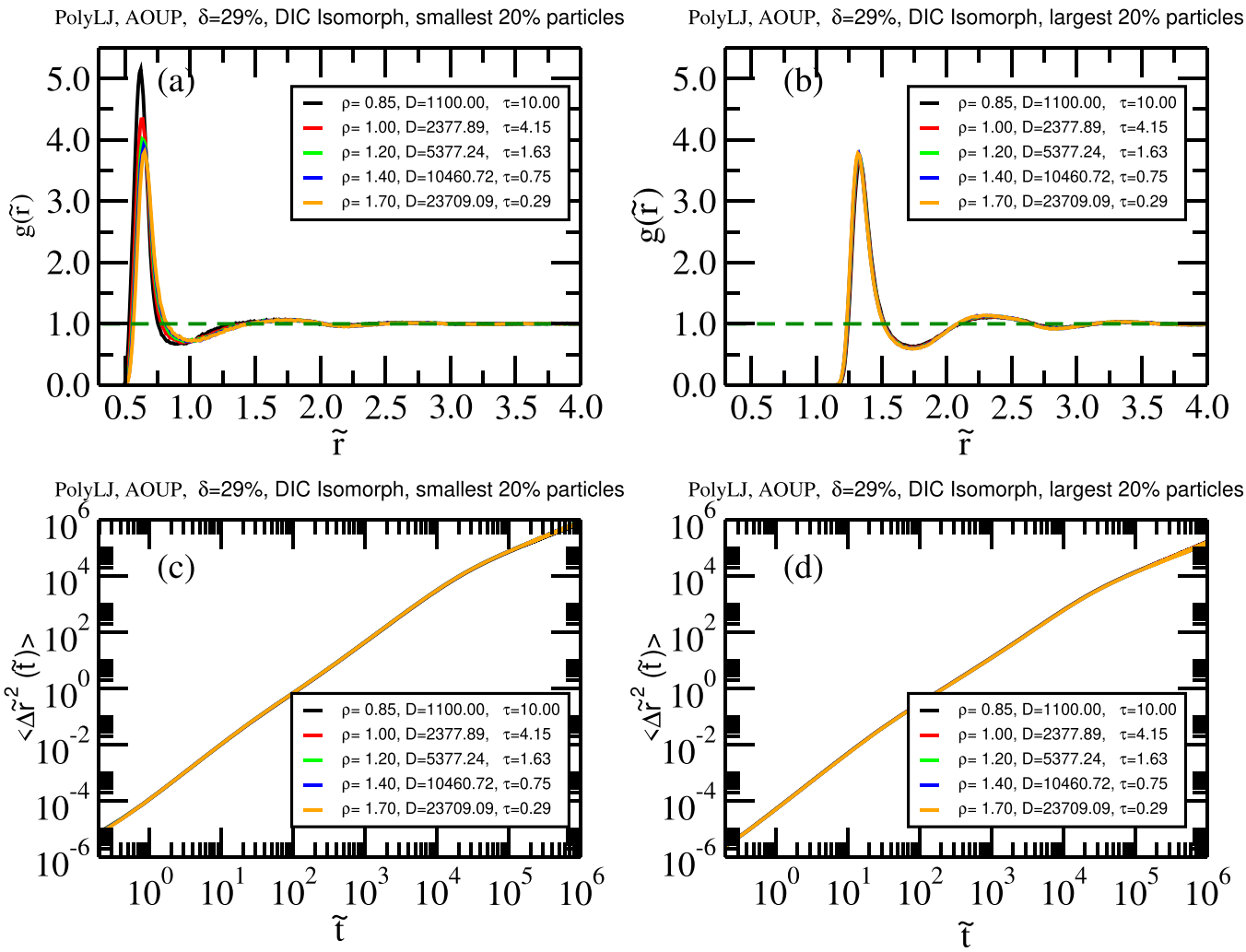

Figure 7. Comparing the degree of invariance of the structure and dynamics of the 20% smallest and largest particles, along the DIC-generated active-matter isomorphs for the $\delta = 29\%$ polydispersity case. (a) and (b) show the reduced RDFs. The invariance of the largest 20% particle RDF is much better than the small-particle RDF. For the MSD, however, both cases are isomorph invariant to a good approximation although the smaller particles move faster than the larger ones.

7. Summary and outlook

We have shown that the uniform-distribution size-polydisperse LJ AOUP model has active-matter isomorphs for the polydispersities $\delta = 12\%$, 23%, and 29%. This demonstrates the robustness of the active-matter-isomorph concept, which for passive systems applies whenever the potential-energy function obeys the hidden-scale-invariance condition discussed in [44, 45]. The existence of isomorphs means that the dimension of the polydisperse AOUP phase diagram is effectively reduced from three to two, because it implies that lines exist in the (ρ, D, τ) phase diagram along which the reduced structure and dynamics are invariant to a good approximation. From a practical perspective, this fact makes it easy to quickly get an overview of the AOUP model's phase diagram.

Two methods have been studied for generating active-matter isomorphs, one based on the configurational temperature and one based on the systemic-temperature concept. We find that both methods work well despite the fact that they do not trace out identical active-matter isomorphs (figure 4). In practice, the latter method will be easier to use in the case of LJ active matter for which a simple expression is available for the function $h(\rho)$ where the parameter γ_0 may be evaluated from a single passive-matter simulation (equation (7)).

More work is needed to clarify how polydispersity relates to the existence of active-matter isomorphs in general. As regards the AOUP model, it would be interesting to investigate whether the introduction of energy polydispersity affects the existence of isomorphs. More generally, other models like the ABP model with a potential-energy function that obeys hidden scale invariance should be investigated in polydisperse versions in order to further illuminate the robustness of the active-matter-isomorph concept.

Data availability statement

All data that support the findings of this study are included within the article.

Acknowledgment

This work was supported by the VILLUM Foundation's *Matter* Grant (16515).

Appendix

This appendix provides more decimals than given in the figures of the parameters ρ, D, and τ used in the simulations. It follows from equations (4) and (9) that both methods for tracing out active-matter isomorphs result in $D\tau\rho^{2/3}$ =Const. Within the number of decimals given, this identity applies for the below reported parameters.

Table S1. Values of D and τ for polydispersity $\delta = 28.87\%$ along the $\rho = 0.85$ isochore (figure 1).

ρ	D	τ
0.8500	1100.0000	10.0000
0.8500	2377.8887	4.1509
0.8500	5377.2401	1.6255
0.8500	10460.7186	0.7540
0.8500	23709.0934	0.2923

Table S2. Values of ρ, D and τ for polydispersity $\delta = 11.55\%$ along the T_{conf} isomorph (figures 2 and 3).

ρ	D	τ
0.9900	1100.0000	10.0000
1.2000	3076.3710	3.1453
1.4000	6577.2502	1.3275
1.7000	16 147.1699	0.4751
2.0000	33 108.2613	0.2079

Table S3. Values of ρ, D and τ for polydispersity $\delta = 23.09\%$ along the T_{conf} isomorph (figures 2 and 3).

ρ	D	τ
0.9050	1100.0000	10.0000
1.1000	3202.8909	3.0155
1.3000	7484.4043	1.1544
1.5000	14 801.2586	0.5306
1.8000	33 821.6367	0.2056

Table S4. Values of ρ, D and τ for polydispersity $\delta = 28.87\%$ along the T_{conf} isomorph (figures 2 and 3).

ρ	D	τ
0.8500	1100.0000	10.0000
1.0000	2704.4638	3.6497
1.2000	6991.3804	1.2502
1.4000	14 743.5375	0.5350
1.7000	35 809.7818	0.1935

Table S5. Values of ρ, D and τ for polydispersity $\delta = 11.55\%$ along the DIC isomorph (figures 5 and 6).

ρ	D	τ
0.9900	1100.0000	10.0000
1.2000	2798.8895	3.4571
1.4000	5629.7965	1.5509
1.7000	13 101.0610	0.5855
2.0000	26 062.3855	0.2641

Table S6. Values of ρ, D and τ for polydispersity $\delta = 23.09\%$ along the DIC isomorph (figures 5 and 6).

ρ	D	τ
0.9050	1100.0000	10.0000
1.1000	2802.7296	3.4460
1.3000	5933.8578	1.4561
1.5000	11 036.5957	0.7116
1.8000	23 877.3029	0.2913

Table S7. Values of ρ, D and τ for polydispersity $\delta = 28.87\%$ along the DIC isomorph (figures 5 and 6).

ρ	D	τ
0.8500	1100.0000	10.0000
1.0000	2377.8887	4.1509
1.2000	5377.2401	1.6255
1.4000	10460.7186	0.7540
1.7000	23709.0934	0.2923

ORCID iDs

Jeppe C Dyre https://orcid.org/0000-0002-0770-5690
Shibu Saw https://orcid.org/0000-0002-6010-2477

References

[1] Mandal R, Bhuyan P J, Chaudhuri P, Dasgupta C and Rao M 2020 Extreme active matter at high densities *Nat. Commun.* **11** 2581
[2] O'Byrne J, Kafri Y, Tailleur J and van Wijland F 2022 Time irreversibility in active matter, from micro to macro *Nat. Rev. Phys.* **4** 167–83
[3] Angelini T E, Hannezo E, Trepat X, Marquez M, Fredberg J J and Weitz D A 2011 Glass-like dynamics of collective cell migration *Proc. Natl Acad. Sci. USA* **108** 4714–9
[4] Marchetti M C, Joanny J F, Ramaswamy S, Liverpool T B, Prost J, Rao M and Simha R A 2013 Hydrodynamics of soft active matter *Rev. Mod. Phys.* **85** 1143–89
[5] Bechinger C, Di Leonardo R, Löwen H, Reichhardt C, Volpe G and Volpe G 2016 Active particles in complex and crowded environments *Rev. Mod. Phys.* **88** 045006
[6] Ramaswamy S 2017 Active matter *J. Stat. Mech.* **2017** 054002
[7] Saintillan D 2018 Rheology of active fluids *Annu. Rev. Fluid Mech.* **50** 563–92
[8] Das M, Schmidt C F and Murrell M 2020 Introduction to active matter *Soft Matter* **16** 7185–90
[9] Shaebani M R, Wysocki A, Winkler R G, Gompper G and Rieger H 2021 Computational models for active matter *Nat. Rev. Phys.* **2** 181–99
[10] Bowick M J, Fakhri N, Marchetti C M and Ramaswamy S 2022 Symmetry, thermodynamics and topology in active matter *Phys. Rev.* X **12** 010501
[11] Marruzzo A, Schirmacher W, Fratalocchi A and Ruocco G 2013 Heterogeneous shear elasticity of glasses: the origin of the boson peak *Sci. Rep.* **3** 1407
[12] Takatori S C and Brady J F 2015 Towards a thermodynamics of active matter *Phys. Rev.* E **91** 032117
[13] Klongvessa N, Ginot F, Ybert C, Cottin-Bizonne C and Leocmach M 2019 Nonmonotonic behavior in dense assemblies of active colloids *Phys. Rev.* E **100** 062603
[14] Buttinoni I, Caprini L, Alvarez L, Schwarzendahl F J and Löwen H 2022 Active colloids in harmonic optical potentials *Europhys. Lett.* **140** 27001
[15] Maggi C, Paoluzzi M, Pellicciotta N, Lepore A, Angelani L and Di Leonardo R 2014 Generalized energy equipartition in harmonic oscillators driven by active baths *Phys. Rev. Lett.* **113** 238303
[16] Farage T, Krinninger P and Brader J M 2015 Effective interactions in active Brownian suspensions *Phys. Rev.* E **91** 042310
[17] Caprini L, Sprenger A R, Löwen H and Wittmann R 2022 The parental active model: a unifying stochastic description of self-propulsion *J. Chem. Phys.* **156** 071102
[18] Maggi C, Marconi U M B, Gnan N and Di Leonardo R 2015 Multidimensional stationary probability distribution for interacting active particles *Sci. Rep.* **5** 10742
[19] Szamel G, Flenner E and Berthier L 2015 Glassy dynamics of athermal self-propelled particles: computer simulations and a nonequilibrium microscopic theory *Phys. Rev.* E **91** 062304
[20] Fodor E, Nardini C, Cates M E, Tailleur J, Visco P and van Wijland F 2016 How far from equilibrium is active matter? *Phys. Rev. Lett.* **117** 038103
[21] Ni R, Stuart M A C and Bolhuis P G 2015 Tunable long range forces mediated by self-propelled colloidal hard spheres *Phys. Rev. Lett.* **114** 018302
[22] Henkes S, Kostanjevec K, Collinson J M, Sknepnek R and Bertin E 2020 Dense active matter model of motion patterns in confluent cell monolayers *Nat. Commun.* **11** 1405
[23] Kumar S, Singh J P, Giri D and Mishra S 2021 Effect of polydispersity on the dynamics of activeBrownian particles *Phys. Rev.* E **104** 024601
[24] Szamel G and Flenner E 2021 Long-ranged velocity correlations in dense systems of self-propelled particles *Europhys. Lett.* **133** 60002
[25] Ninarello A, Berthier L and Coslovich D 2017 Models and algorithms for the next generation of glass transition studies *Phys. Rev.* X **7** 021039
[26] Abraham S E, Bhattacharrya S M and Bagchi B 2008 Energy landscape, antiplasticization and polydispersity induced crossover of heterogeneity in supercooled polydisperse liquids *Phys. Rev. Lett.* **100** 167801
[27] Zaccarelli E, Liddle S M and Poon W C K 2015 On polydispersity and the hard sphere glass transition *Soft Matter* **11** 324
[28] Pihlajamaa I, Laudicina C C L and Janssen L M C 2023 Polydispersity modifies relaxation mechanisms in glassy liquids (arXiv:2302.09549)
[29] Caprini L, Marconi U M B, Maggi C, Paoluzzi M and Puglisi A 2020 Hidden velocity ordering in dense suspensions of self-propelled disks *Phys. Rev. Res.* **2** 023321
[30] Keta Y-E, Jack R L and Berthier L 2022 Disordered collective motion in dense assemblies of persistent particles *Phys. Rev. Lett.* **129** 048002
[31] Gnan N, Schrøder T B, Pedersen U R, Bailey N P and Dyre J C 2009 Pressure-energy correlations in liquids. IV. 'Isomorphs' in liquid phase diagrams *J. Chem. Phys.* **131** 234504
[32] Saw S, Costigliola L and Dyre J C 2023 Configurational temperature in active matter. I. Lines of invariant physics in the phase diagram of the Ornstein–Uhlenbeck model *Phys. Rev.* E **107** 024609
[33] Saw S, Costigliola L and Dyre J C 2023 Configurational temperature in active matter. II. Quantifying the deviation from thermal equilibrium *Phys. Rev.* E **107** 024610
[34] Ingebrigtsen T S, Schrøder T B and Dyre J C 2021 Hidden scale invariance in polydisperse mixtures of exponential repulsive particles *J. Phys. Chem.* B **125** 317–27

[35] Toxvaerd S and Dyre J C 2011 Communication: shifted forces in molecular dynamics *J. Chem. Phys.* **134** 081102
[36] Bailey N P *et al* 2017 RUMD: a general purpose molecular dynamics package optimized to utilize GPU hardware down to a few thousand particles *Scipost Phys.* **3** 038
[37] Landau L D and Lifshitz E M 1958 *Statistical Physics* (Pergamon Press)
[38] Rugh H H 1997 Dynamical approach to temperature *Phys. Rev. Lett.* **78** 772–4
[39] Powles J G, Rickayzen G and Heyes D M 2005 Temperatures: old, new and middle aged *Mol. Phys.* **103** 1361–73
[40] Bøhling L, Ingebrigtsen T S, Grzybowski A, Paluch M, Dyre J C and Schrøder T B 2012 Scaling of viscous dynamics in simple liquids: theory, simulation and experiment *New J. Phys.* **14** 113035
[41] Ingebrigtsen T S, Bøhling L, Schrøder T B and Dyre J C 2012 Thermodynamics of condensed matter with strong pressure-energy correlations *J. Chem. Phys.* **136** 061102
[42] Bailey N P, Pedersen U R, Gnan N, Schrøder T B and Dyre J C 2008 Pressure-energy correlations in liquids. I. Results from computer simulations *J. Chem. Phys.* **129** 184507
[43] Dyre J C 2020 Isomorph theory beyond thermal equilibrium *J. Chem. Phys.* **153** 134502
[44] Schrøder T B and Dyre J C 2014 Simplicity of condensed matter at its core: generic definition of aRoskilde-simple system *J. Chem. Phys.* **141** 204502
[45] Dyre J C 2018 Perspective: excess-entropy scaling *J. Chem. Phys.* **149** 210901